China Geology 7 (2024) 702−713

China Geology

Journal homepage: http://chinageology.cgs.cn
https://www.sciencedirect.com/journal/china-geology

Molecular structure characterization of middle-high rank coal via ^{13}C NMR, XPS, and FTIR spectroscopy

Xiao-ming Ni[a], Jing-shuo Zhang[a], Xiao-kai Xu[a], Bao-yu Wang[b]

[a] *School of Energy Science and Engineering, Henan Polytechnic University, Jiaozuo* 454000, *China*
[b] *Institute of Resources & Environment, Henan Polytechnic University, Jiaozuo* 454000, *China*

ARTICLE INFO

Article history:
Received 2 November 2021
Received in revised form 1 March 2022
Accepted 13 April 2022
Available online 25 January 2024

Keywords:
Molecular structure model
Carbon-13 nuclear magnetic resonance (NMR)
X-ray photoelectron spectroscopy (XPS)
Fourier transform infrared spectroscopy (FTIR)
Coal

ABSTRACT

Elemental analysis, nuclear magnetic resonance carbon spectroscopy (^{13}C-NMR), X-ray photoelectron spectroscopy (XPS) and Fourier transform infrared spectroscopy (FTIR) experiments were carried out to determine the existence of aromatic structure, heteroatom structure and fat structure in coal. MS (materials studio) software was used to optimize and construct a 3D molecular structure model of coal. A method for establishing a coal molecular structure model was formed, which was "determination of key structures in coal, construction of planar molecular structure model, and optimization of three-dimensional molecular structure model". The structural differences were compared and analyzed. The results show that with the increase of coal rank, the dehydrogenation of cycloalkanes in coal is continuously enhanced, and the content of heteroatoms in the aromatic ring decreases. The heteroatoms and branch chains in the coal are reduced, and the structure is more orderly and tight. The stability of the structure is determined by the π-π interaction between the aromatic rings in the nonbonding energy E_N. Key Stretching Energy The size of E_B determines how tight the structure is. The research results provide a method and reference for the study of the molecular structure of medium and high coal ranks.

1. Introduction

The establishment of the molecular structure model of coal can lay a foundation for explaining the microscopic adsorption mechanism of coal (Xie HP et al., 2018). In the early stage of the study, researchers obtained information pertaining to the coal molecular structure using chemical experimental methods such as pyrolysis and condensation polymerization, thus establishing a planar molecular model. Among them, the classical coal planar molecular structure models include the Fuchs model, Given model, Wiser model, and Shinn model (Chermin HAG et al., 1957; Given PH et al., 1960; Wiser WH et al., 1975; Shinn JH et al., 1984). The Fuchs model is a model constructed by statistical structural analysis. The Given model is constructed based on infrared spectroscopy and X-ray diffraction (XRD) experiments, but does not consider sulfur atoms, ether bonds, *etc*. In the Wiser model, sulfur atoms are taken into account, but surface functional groups, fatty side chain structures, and the stability of condensed aromatic ring in three-dimensional space are not considered. In the Shinn model, the occurrence forms of sulfur, nitrogen, and other heteroatoms are considered, and the low-coal rank molecular model is constructed.

In recent years, modern test and analysis techniques and computer-aided molecular design (CAMD) techniques have been widely used in the construction of molecular structure models of coal. The molecular structure model of coal develops gradually from plane structures to a three-dimensional structure. Zhou Z et al., (2020) used industrial analysis, elemental analysis, ^{13}C NMR, XPS, and FTIR methods to study the forms of aromatic ring, aliphatic atoms, and oxygen atoms, and establish the macromolecular structure of vitelite organic matter. Surip SN et al., (2020) observed the surface morphology of Malaysia SAMKC low-coal rank by scanning electron microscope (SEM), studied its crystal structure by XRD, identified the functional groups on the coal surface by FTIR (Perkin-Elmer, Spectrum Rx I), and explored the adsorption characteristics of coal. Jiang JY et al., (2019) used XRD, Raman spectroscopy and FTIR to characterize the coalification of middle and high coal rank specimens. Jawad

First author: *E-mail address*: nxm1979@126.com (Xiao-ming Ni).

Literary editor: Li-qiong Jia
doi:10.31035/cg2022135
2096-5192/© 2024 China Geology Editorial Office.

AH et al., (2019) used pore structure analysis (BET), scanning electron microscopy with energy dispersive X-ray spectroscopy (SEM-EDX), XRD, FTIR, elemental analysis (CHNS), thermogravimetric analysis (TGA), and the method for determination of the point of zero charge (pHPZC) to characterize the adsorption properties and energy composition of Malaysian Selantik low-rank coal specimens. Song Y et al., (2017) used ^{13}C NMR, FTIR, and HRTEM analysis and testing techniques to study the microstructure of vitrinite coal and discuss the adsorption characteristics of CH_4.

In order to sort out the relationship between the experimental test data and the coal molecular structure model more clearly, and optimize the three-dimensional structure model of coal molecules, this paper takes the medium-high metamorphic degree coal in Pingdingshan No. 6 Mine, Hebi No. 4 Mine, Xiegou Mine, Changping Mine, Sihe Mine and other mines as the research object, adopts the analysis and detection technology of elemental analysis + FTIR + ^{13}CNMR + XPS, and applies the Origin peak fitting technology and the principle of energy minimum. Determination of key structures in coal, construction of planar molecular structure model, optimization of three-dimensional molecular structure model", and the differences in molecular structure of coal with medium to high metamorphic degree were compared and analyzed. The research results provide a model basis for the study of the evolution process and mechanism of molecular structure of coal with medium and high metamorphic degrees.

2. Experimental work

2.1. Materials

Following regulations in Sampling of Coal Seams (GB/T 482-2008, 2008), coal samples were taken from Xiegou (XG) Mine, Changping (CP) Mine, and Sihe (SH) Mine in Shanxi Province, China and the No. 4 Mine of the Hebi (HB) Mining Area and No. 6 Mine of the Pingdingshan (PDS) Mining Area in Henan Province, China and sealed in collection bags.

The collected coal samples were ground to pass a 200 mesh. Elements such as C, H, O, N, and S in the coal were detected using an elemental analyzer in accordance with the *Calibration Specification for Elemental Analyzers* (Metrological Specifications of the People's Republic of China, 2011). The *Method of Determining Microscopically the Reflectance of Vitrinite in Coal* (GB 6948-2008, 2008) was followed to test the vitrinite reflectance (*R*o, max) of the coal; coal ranks were classified according to ISO11760 standards (Table 1).

It can be seen from Table 1 that PDS and HB coal samples were middle coal rank; XG, CP, and SH coal samples were high coal rank. Proportions of elements C, H, N, O, and S in the coal samples were separately in the ranges of 88.25% –91.06%, 3.13%–4.29%, 1.58%–1.91%, 3.71%–5.34%, and 0.37%–0.52%. Among them, the proportion of C was used as one of the standards with which to grade the rank of each coal; H and O had approximately equal proportions; while the proportion of S was the lowest, at less than 1%.

2.2. Optimized modeling method for molecular structures

The optimized stereoscopic model for molecular structures in coal with moderate and high degrees of metamorphism was established by combining test techniques such as the ^{13}C NMR (Liu Y et al. 2017; Ping A et al. 2020; Xiang JH et al. 2016; Yan J et al. 2020), elemental analysis, XPS, and FTIR with Materials Studio (MS) software. The specific method is shown as follows:

(1) Identifying forms of aromatic hydrocarbons in coal samples by combining ^{13}C NMR with elemental analysis results;

(2) Determining forms of aliphatic hydrocarbons in coal samples by integrating FTIR with ^{13}C NMR;

(3) Calculating forms of heteroatoms in coal samples by combining the XPS with the elemental analysis results;

(4) Establishing a planar model for molecular structures in coal by combining ACD/CNMR predictor with the ^{13}C NMR; optimizing the planar macromolecular structures using the molecular mechanics and molecular dynamics (annealing kinetics) modules in the MS software.

2.2.1. Analysis and testing of aromatic hydrocarbons

Aromatic hydrocarbons comprise the main molecular structures in coal. A ^{13}C NMR spectrometer is one of the more commonly used test instruments when studying molecular structures in coal. Methods for determining forms of aromatic hydrocarbons in coal are described as follows:

(i) Demineralization of coal samples

Demineralization was used to remove clay minerals and impurities from a coal: Pulverized coal was screened by using a 200-mesh standard sieve and then 10 g samples were weighed and dried under vacuum at 80°C for 2 h. Thereafter, 5 g of each dried coal sample could be put in a tetrafluoroethylene beaker, in which 30 mL of 37% (mass fraction) hydrochloric acid and 20 mL of 40% (mass fraction)

Table 1. Test results of contents of main elements and Rmax in coal samples.

Coal sample	Serial number	Rmax/%	Elemental analysis						
			C/%	H/%	N/%	O/%	S/%	H/C	O/C
Pingdingshan Six Mine Coal	PDS	1.28	88.98	3.88	1.82	4.82	0.50	0.52	0.04
Hebi Four Mine Coal	HB	1.78	88.25	4.29	1.66	5.34	0.46	0.58	0.05
Xiegou Mine Coal	XG	2.04	89.25	4.05	1.73	4.60	0.37	0.54	0.04
Changping Mine Coal	CP	2.68	88.91	3.77	1.91	4.98	0.43	0.51	0.04
Sihe Mine Coal	SH	3.28	91.06	3.13	1.58	3.71	0.52	0.41	0.03

Note: Rmax is the average maximum vitrinite reflectance of coal. 0.5%≦Rmax<2% is the top coal rank (Bituminous coal); 2%≦Rmax<6% is the high coal rank (Anthracite coal).

hydrofluoric acid were slowly added. Then the mixture was stirred magnetically at 60°C for 8 h, followed by three pickling cycles. The coal samples, after pickling, were then centrifuged and washed with deionized water until their pH was neutral (as evinced by the use of pH test strips). After being oven-dried at 60°C for 8 h, the samples were removed for later use.

(ii) ^{13}C NMR

A Bruker 600-MHz NMR spectrometer with superconducting magnet coils and double-resonance solid-state probes was used; the device was equipped with ZrO_2 rotors with an outer diameter of 4 mm. The magic-angle spinning frequency was 10 kHz and the resonant frequency of the ^{13}C nucleus was 151.1 MHz. The sampling lasted for 0.02 s, with the cyclic delay time, pulse width, and number of scans of 3 s, 4 μs, and 6000, respectively. The cross-polarization/magic-angle spinning (CP/MAS) technique was used, with a contact time of 2 ms and tested spectral width (SW) of 300×10^{-6}.

(iii) Aromatic hydrocarbons

The method for determining aromatic hydrocarbons present in coal is as follows:

Step 1: The ^{13}C-NMR parameters are obtained by the peak fitting was carried out by Origin.

Step 2: The ratio of bridging aromatic C to peripheral C pertaining to the tested coal samples is calculated using Formula (1):

$$X_{BP} = f_a^B \Big/ \left(f_a^S + f_a^P + f_a^H\right) \tag{1}$$

where X_{BP} represents the ratio of aromatic bridgehead C to aromatic peripheral C on aromatic rings; f_a^B, f_a^S, f_a^P, and f_a^H denote aromatic bridgehead C, alkylated aromatic C, aromatic C bonded to hydroxyl or ether oxygen, and protonated and aromatic C, respectively.

2.2.2. Analysis and testing of aliphatic hydrocarbons

The determination of aliphatic hydrocarbons in coal is mainly by FTIR and ^{13}C-NMR methods:

(i) FTIR

An IS50-Thermo Fisher infrared spectrometer was adopted to perform the FTIR test on the coal samples following the *General Rules for Infrared Analysis* (GB/T 6040-2002 et al., 2002).

(ii) Aliphatic hydrocarbons

Step 1: Previous research has revealed that peaks (Han F et al. 2014; Zhao YG et al. 2018; Ge T et al. 2020; Hao PY et al. 2020) at 700–900 cm^{-1}, 1000–1800 cm^{-1}, 2800–3000 cm^{-1}, and 3100–3650 cm^{-1} are absorption peaks of aromatic hydrocarbons, O- and S-containing heteroatomic functional groups, aliphatic hydrocarbons, and hydroxyls, respectively. Based on the research results, spectrum segmentation and peak fitting are conducted, thus obtaining the assignment and proportion of peaks for each functional group and structure.

Step 2: By using f_{al}^* (CH_3 or quaternary C) and f_{al}^H (CH or CH_2) data in the ^{13}C NMR parameters and combining with the assignment and proportion of peaks for aliphatic hydrocarbons on the FTIR spectra, the main structural forms thereof can be obtained.

Step 3: The number of C atoms in aliphatic hydrocarbons can be derived using Formulae (2) and Formulae (3). In this way, the main forms of aliphatic hydrocarbons present in each specimen are ascertained.

$$A = a/f_a' \tag{2}$$

$$b = A - a \tag{3}$$

where a represents the number of aromatic C atoms and f_a' refers to the proportion of aromatic C; A and b denote the total number of C atoms and the number of aliphatic C atoms, respectively.

2.2.3. Analysis and testing of heteroatoms

The specific methods of determination are as follows:

(i) XPS

An AXIS ULTRA DLD X-ray photoelectron spectrometer was used to perform XPS on the coal samples based on the *General Rules for X-Ray Photoelectron Spectroscopic Analysis Method* (GB/T19500-2004 et al., 2004). The transmission capacities during full scanning and narrow scanning using the spectrometer were 160 eV in increments of 1 eV and 40 eV in increments of 0.05 eV, under a base vacuum of 5×10^{-9} Pa.

(ii) Heteroatoms

Step 1: Previous research has proved that C is present in four forms in molecular structures of coal (Kozlowski M, 2004): The peaks at binding energy of 284.48 eV and 285.22 eV are assigned to aromatic and graphitized C (C-C) and C-H structures; the peak at 286.53 eV is ascribed to C bonded to phenol or ether oxygen (C-O); and the peak at 287.61 eV is assigned to carbonyl (C=O). O appears in three forms: The peak at 531.90 eV corresponds to phenolic hydroxyl groups and ether-oxygen bonds (C-O), peaks at 532.34 eV and 533.34 eV are ascribed to carbonyls (C=O), and the peak at 534.35 eV is assigned to carboxyl (COOH). As for N, it is present in four forms: The peaks at 398.06 eV, 399.96 eV, 401.37 eV, and 402.89 eV separately correspond to pyridine N, pyrrole N, quaternary N, and oxynitride. S is mainly found to exist in five forms: The peaks at 163.54 eV, 164.57 eV, 167.03 eV, 168.66 eV, and 170.31 eV are ascribed to mercaptan and thiophenol, thiophenic S, sulfoxide S, sulfone S, and inorganic S, respectively. According to these results and through peak fitting, the assignment and proportion of structural forms of each atom are determined.

Step 2: The numbers of each atom are calculated using Formulae (4) and Formulae (5) according to the results of elemental analysis. The main structural forms of heteroatoms are attained by analyzing XPS data, in which

$$B = A/\alpha \tag{4}$$

$$c = \eta B \tag{5}$$

where B and c separately refer to the total number of atoms and the number of a certain heteroatom; η represents the proportion of a certain heteroatom in the elemental analysis (Table 1); α represents the proportion of C atoms in Table 1.

2.2.4. Methods for constructing macromolecular structure models

The specific methods include:

(i) Drawing of planar macromolecular structures and verification of calculated results

Step 1: According to the determined forms of aromatic hydrocarbons, aliphatic hydrocarbons, and heteroatoms in the coal samples, their chemical structures are obtained and drawn using the ACD/ChemSketch software.

Step 2: Chemical shifts of the drawn planar structures are calculated using ACD/CNMR predictor, thus attaining the ^{13}C NMR spectra, which are then imported into Origin software for comparisons with the experimental spectra to verify the accuracy of the calculated ^{13}C NMR spectra.

(ii) Model optimization

To make the established molecular structure model of coal better resemble the actual structures, molecular mechanics and molecular dynamics (annealing kinetics) in MS were used to optimize the planar macromolecular structures. Specific parameter settings: Dreiding was selected as the force field in the simulation study, and the charge balance method (Q_{eq} method) was used as the charge method. The Ewald summation method was used for electrostatic action with the accuracy of 1×10^{-5} kcal/mol. Van der Waals interaction and hydrogen bonding were truncated at 2.3 nm and 0.1 nm using an atom-based method. To allow the system to equilibrate, 2×10^{6} Monte Carlo steps were used in each simulation, among which the first 10^{6} Monte Carlo steps were adopted to reach equilibrium, and the last 10^{6} Monte Carlo steps were used to calculate the required physical quantities by statistical averaging. The average value of three parallel calculations was used to obtain the result, and the control coefficient of variation was within 0.01. The dynamics of the Forcite module in the software was used for the calculation of Molecular dynamics (MD). The adsorption locator module in the simulation application software was conducted. This module adopted the principle of simulated annealing to determine the adsorption site according to energy minimization. The optimal adsorption configuration obtained by the GCMC method was used as the initial configuration for molecular dynamics simulation. The initial rate followed the Boltzmann random distribution, and the canonical (NVT) ensemble was used. The temperature of Nose was 298.15 K in the Dreiding field temperature-control method. The simulation time was 3000 ps, the step size was 0.5 fs, and the output was provided once every 100 steps. The first 1500 ps was used to balance the system, and the last 1500 ps was used to calculate the structure and dynamic properties of the system.

3. Results and discussion

3.1. Coal property analysis

3.1.1. Determination of forms of aromatic hydrocarbons

(i) Test results of ^{13}C NMR parameters based on the ^{13}C CP/MAS spectra

The ^{13}C NMR spectra obtained in the test were subjected to peak fitting to determine peak positions and relative percentages of different C atoms (Fig. 1).

Figs. 1a–e separately depict the spectra of PDS, HB, XG, CP, and SH coal samples after peak fitting. Fig. 1f compares the overall spectra of the five coal samples. From the left-hand side to the right-hand side, there are three distinct C

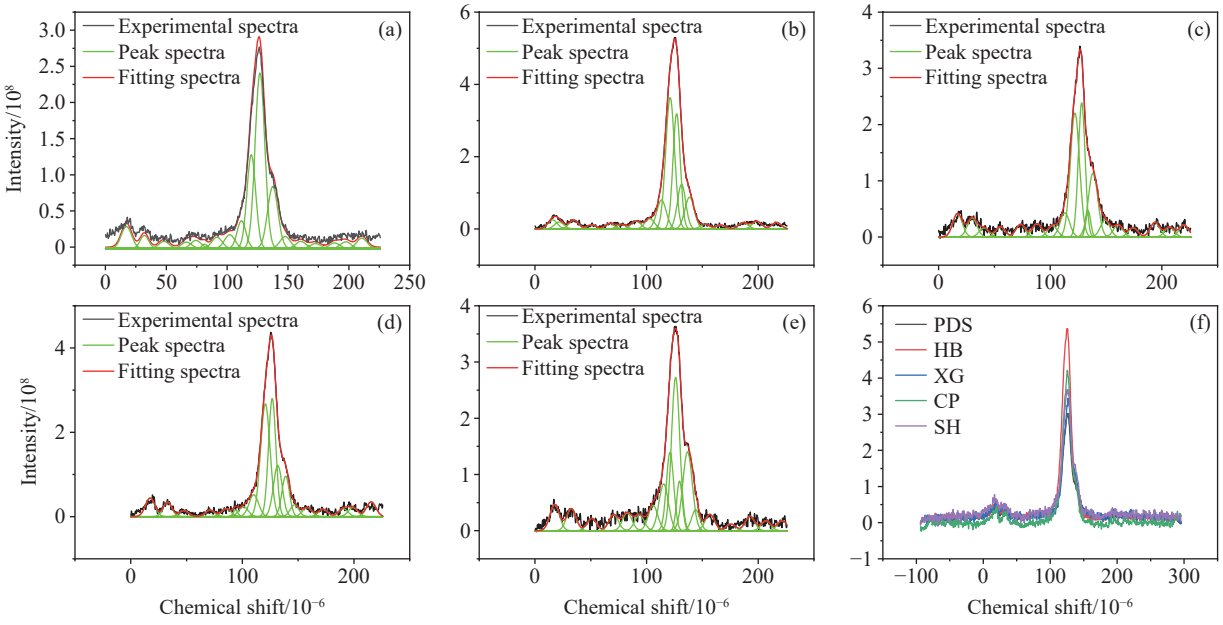

Fig. 1. Peak fitting ^{13}C CP/MAS spectra. a–PDS Coal; b–HB Coal; c-XG Coal; d-CP Coal; e-SH Coal; f-Compares the overall spectra of the five coal samples.

Table 2. Table of ^{13}C NMR chemical displacement attribution.

Peak sequence number	Peak type	Fitting peak area	FWHM	Maximum height	Peak weighted average center	Percentage of fitting peak area/%	Peak attribution
1	Gaussian	3.51E+08	10.00	3.29E+07	17.27	4.82	Lipo methyl
2	Gaussian	1.72E+08	8.23	1.96E+07	31.99	2.36	methylene
3	Gaussian	1.13E+08	10.00	1.06E+07	48.16	1.55	Submethyl, quaternary carbon
6	Gaussian	1.02E+08	10.00	9.55E+06	66.61	1.40	Oxygenated methylene carbon
5	Gaussian	1.30E+08	10.00	1.22E+07	74.34	1.79	Oxygenated methylene carbon
4	Gaussian	3.35E+07	5.00	6.29E+06	81.48	0.46	Epoxy resin carbon
7	Gaussian	1.79E+08	10.00	1.68E+07	91.61	2.46	Epoxy resin carbon
9	Gaussian	2.20E+08	10.00	2.06E+07	102.12	3.02	Protonated aromatic carbon
8	Gaussian	3.76E+08	8.46	4.18E+07	111.80	5.17	Protonated aromatic carbon
10	Gaussian	1.27E+09	8.49	1.40E+08	119.87	17.42	Protonated aromatic carbon
11	Gaussian	2.60E+09	9.27	2.63E+08	126.97	35.74	Protonated aromatic carbon
12	Gaussian	9.89E+08	10.00	9.29E+07	137.49	13.60	Bridged aromatic carbon
13	Gaussian	1.91E+08	10.00	1.80E+07	147.68	2.63	Side branch aromatic carbon
14	Gaussian	1.13E+08	10.00	1.06E+07	160.54	1.55	Oxygen replaces aromatic carbon
15	Gaussian	7.81E+07	10.00	7.33E+06	172.50	1.07	carbonyl-c
16	Gaussian	8.88E+07	10.00	8.34E+06	188.26	1.22	carbonyl-c
17	Gaussian	1.07E+08	10.00	1.01E+07	197.52	1.48	carbonyl carbon
18	Gaussian	1.63E+08	10.00	1.53E+07	210.68	2.25	carbonyl carbon

Table 3. Table of ^{13}C NMR parameters.

Coal sample number	X_{BP}	f_a/%	f_a'/%	f_a^H/%	f_a^N/%	f_a^P/%	f_a^S/%	f_a^B/%	f_a^C/%	f_{al}/%	f_{al}^*/%	f_{al}^H/%	f_{al}^O/%
PDS	0.21	85.15	79.14	61.36	17.78	1.55	2.63	13.60	6.02	14.85	4.82	7.10	2.92
HB	0.27	88.12	82.91	62.92	20.00	0.98	1.21	17.81	5.21	11.88	4.05	3.31	4.51
XG	0.27	82.00	72.80	51.25	21.55	2.47	3.43	15.65	9.20	18.00	4.79	7.87	5.34
CP	0.31	86.93	77.78	54.70	23.08	2.13	2.51	18.44	9.15	13.07	4.35	4.55	4.17
SH	0.36	80.33	73.25	47.68	25.57	2.93	3.22	19.42	7.08	19.67	4.68	6.15	8.84

Notes: f_a–total sp^2 hybridized C; f_{al}–total sp^3hybridized C; f_a^C–carbonyl group or carboxyl group C (δ>165); f_a'–aromatic C; f_a^H–protonated and aromatic C (δ=100–129); f_a^N–nonprotonated and aromatic C; f_a^P–aromatic C bonded to hydroxyl or ether oxygen (δ=152–165) ; f_a^S–alkylated aromatic C (δ=139–152); f_a^B–aromatic bridgehead C (δ=129–139); f_{al}^*–CH_3 or quaternary C(δ=16); f_{al}^H–CH or CH_2(δ=30); f_{al}^O–aliphatic C bonded to oxygen (δ=75–90).

peaks in the overall spectra, which correspond to aliphatic C, aromatic C, and carbonyl C, separately.

Based on peak-fitting the data for the ^{13}C CP/MAS NMR spectra in Fig. 1, the attribution of peak locations was analyzed and listed in Table 2 (taking PDS as an example).

By analyzing the spectra after peak fitting, the ^{13}C NMR parameters are identified (Table 3).

(ii) Determination of forms of aromatic hydrocarbons in coal exhibiting different degrees of metamorphism

It is calculated, using Formula (1), that the ratios of aromatic bridgehead C to aromatic peripheral C in the PDS, HB, XG, CP, and SH coal samples are 0.21, 0.27, 0.27, 0.31, and 0.36, respectively. When the C content in coal was 83%–90%, there are, on average, three to five rings in the aromatic planes. According to Table 3, the main forms of aromatic hydrocarbons in each coal sample were determined (Table 4). In accordance with the numbers of aromatic C atoms in each coal sample, the total number of C atoms was calculated using Formula (2), as shown in Table 4.

The Table 4 shows that structures of aromatic rings become more compact with increasing coal rank.

3.1.2. Determination of forms of aliphatic hydrocarbons

Absorption peaks on the infrared spectra of coal can be classified into one of four types: Absorption peaks of aromatic hydrocarbons, O and S-containing heteroatomic functional groups, aliphatic hydrocarbons, and hydroxyls. Peak fitting was performed for these four types of absorption peaks for the five types of coal samples (Li XZ et al., 2015; Li W et al., 2016; Liu WY et al., 2019; Liu BJ et al., 2022; Jia TG et al., 2021). Spectra of PDS coal samples were taken as an example (Fig. 2).

By analyzing spectral data after peak fitting, the chemical structures and assignment data of the four types of absorption peaks on the infrared spectra were obtained. Table 5 only lists data pertaining to those aromatic hydrocarbons needed for

modeling. Data associated with aliphatic hydrocarbons are shown in Table 6.

The number of aliphatic C atoms was calculated using Formula (3). Then, the numbers of CH_3, CH_2, and CH in each coal sample were computed according to proportions of f_{al}^H *and* f_{al}^* showing the ^{13}C NMR results, and relative proportions of CH_3, CH_2, and CH in Table 6 are combined.

Table 4. Main forms of aromatic hydrocarbons in each coal sample.

Coal sample	Chemical structure				
	PDS	HB	XG	CP	SH
	1	—	—	—	—
	5	11	11	8	5
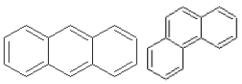	—	2	2	1	5
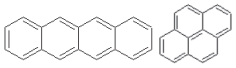	—	—	—	2	1
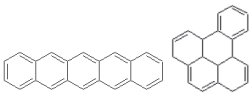	—	—	—	—	1
Number of aromatic carbon atoms	56	138	138	130	160
Total carbon atoms	71	166	190	167	218

The results are listed in Table 7.

It can be seen from Fig. 3 and Fig. 4 that with the increase of coal metamorphism, the proportion of multi-substituted aromatic rings decreased. Monozoal aromatic rings that accounted for 11.81% overall appeared in SH anthracite, indicating that the higher substituted aromatic rings tended to move to the middle and lower substituted aromatic rings. With the increase of coal rank, the CH content decreased from 27.27% to 16.24%, the CH_2 content increased from 24.32% to 31.18%, and the CH_3 content increased from 48.41% to 52.58%. This phenomenon was mainly caused by the cyclization of the aliphatic chain, aromatization of the cycloalkane, substitution of the locator group on the aromatic ring, and decarboxylation of the aromatic ring.

3.1.3. Determination of structural forms of heteroatoms

The results of peak fitting of C, O, N, and S in X-ray photoelectron spectra in coal and those of PDS coal samples were taken as an example (Fig. 5).

The assignment and proportions of peaks at each binding energy were attained by analysis of the data (Table 8).

Table 8 indicates that among the heteroatoms, O atoms were mainly present in the form of C-O, along with some C=O and OH^-, in a ratio of approximately 2∶1∶1. The main forms of N atoms included: in PDS and CP coal samples, N atoms mainly appeared as pyrrole and pyridine N; those in HB samples were mainly present as pyrrole and quaternary N; in XG and SH samples, pyridine N and oxynitride were found to be the main forms of N. In terms of S atoms, they were

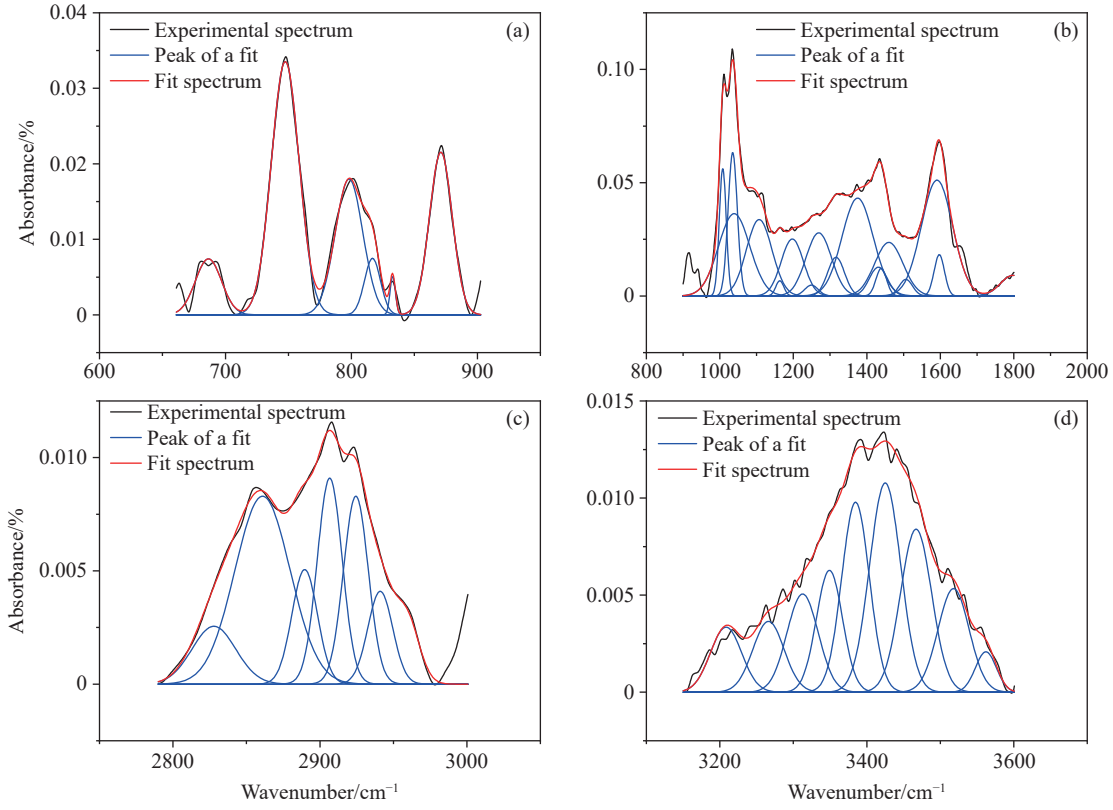

Fig. 2. Peak fitting FTIR spectra of PDS. a–Peak fitting of aromatic hydrocarbons spectra; b–peak fitting of oxygen-containing functional groups; c–peak fitting of aliphatic hydrocarbons spectra; d–peak fitting of hydroxyl hydrogen bond spectra.

Table 5. Aromatic hydrocarbons chemical structures and assignment data.

Coal sample number	Monosubstituted aromatic rings/%	Disubstituted aromatic rings/%	Tri-substituted aromatic rings/%	Tetrasubstituted aromatic rings/%	Five substituted aromatic rings/%
PDS	-	45.04	24.04	7.12	23.81
HB	-	42.52	6.77	25.17	25.53
XG	-	12.69	31.89	3.34	20.47
CP	-	13.74	58.10	6.28	21.88
SH	11.81	37.30	29.49	7.26	14.15

Table 6. Aliphatic hydrocarbons chemical structures and assignment data.

Coal sample number	methyl symmetric stretching vibration/%	methylene antisymmetric stretching vibration/%	methyl antisymmetric stretching vibration/%	methyne stretching vibration/%	methylene symmetric stretching vibration/%
PDS	35.02	15.83	13.39	27.27	8.49
HB	31.08	27.52	16.44	15.63	9.33
XG	37.00	22.19	10.39	21.48	8.94
CP	22.36	24.08	21.33	17.82	14.41
SH	36.74	20.26	15.84	16.24	10.92

Table 7. Main forms of aliphatic hydrocarbons.

Coal sample number	CH_3	CH_2	CH	Number of aliphatic carbon atoms
PDS	7	4	4	15
HB	14	10	4	28
XG	25	16	11	51
CP	16	14	7	37
SH	31	18	9	58

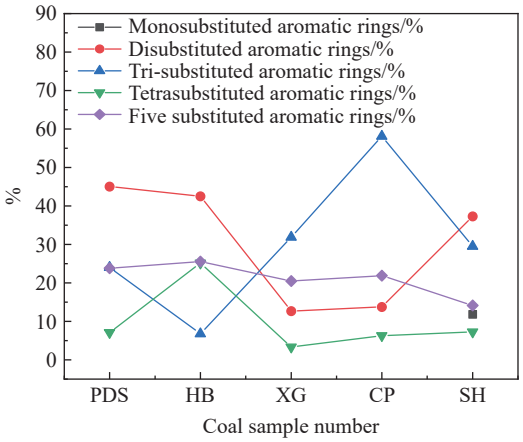

Fig. 3. Chemical structure changes of aromatic hydrocarbons.

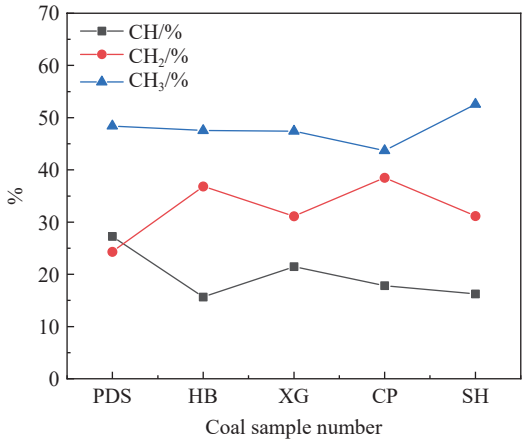

Fig. 4. Chemical structure changes of aliphatic hydrocarbons.

mainly thiophenic and inorganic S in PDS and XG samples, mercaptan and thiophenol in HB samples, thiophenic and sulfoxide S in CP samples, and mercaptan, thiophenol, and sulfoxide S in SH samples, respectively.

According to Formulae (4) and Formulae (5), the numbers of heteroatoms O, N, and S atoms were calculated. As the proportion of S was only 0.37%–0.52%, the element was ignored. The chemical structures formed by heteroatoms were determined using proportions listed in Table 8 and the main forms of the heteroatomic structures are shown in Table 9.

3.1.4. Establishment and optimization of the macromolecular structure model

(i) Drawing of planar macromolecular structures and verification of calculated results

The ACD/ChemSketch software was used to draw the planar model of the molecular structures in these coals. The chemical shifts of the structure model were calculated using the ACD/CNMR predictor. In this way, the ^{13}C NMR spectra were calculated (Grzybek T et al. 2002). The calculated and tested ^{13}C NMR spectra are illustrated in Fig. 6.

The authors continued to modify the structure until it was closest to the measured element content and nuclear magnetic spectrum (Table 10).

To verify the correctness of the model, the simulated data were compared with the experimental data. Fig. 6 shows the comparison between the plane model spectrum and the solid nuclear magnetic spectrum of anthracite: The nuclear magnetic spectrum of anthracite plane model was consistent with the solid nuclear magnetic spectrum of the above experiment. Through inversion of the model output, the element content of anthracite was obtained, which was very close to the element analysis results pertaining to previous experimental coal samples and consistent with the range of element contents of anthracite as predicted theoretically (Table 10).

(ii) Model optimization

The model was optimized using the proposed optimization

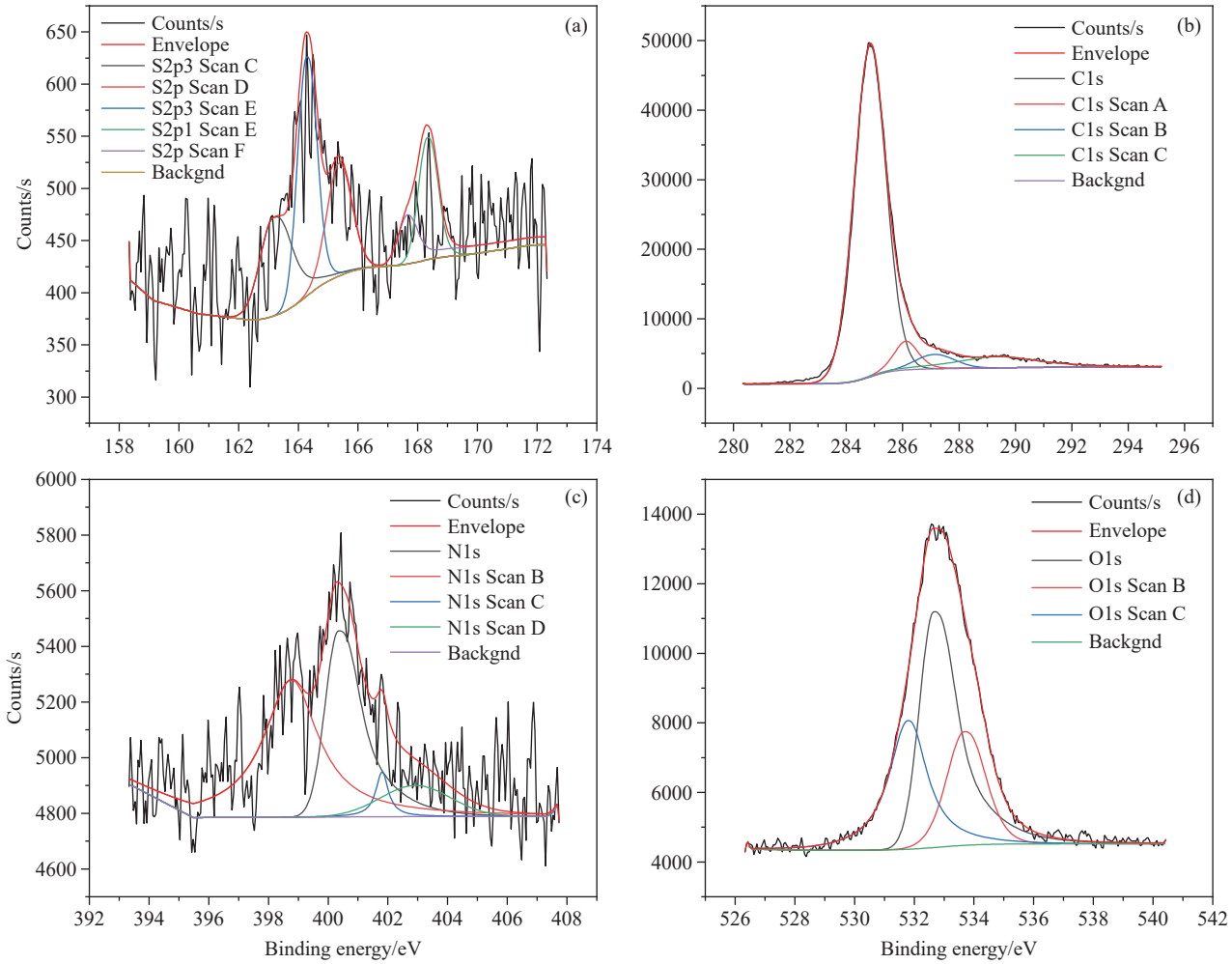

Fig. 5. Peak fitting binding energy spectra of PDS. a–peak fitting of S spectra; b–peak fitting of C spectra; c–peak fitting of N spectra; d–peak fitting of O spectra.

Table 8. Assignment and proportions of peaks at each binding energy.

Test type	eV	assignment	PDS	HB	XG	CP	SH
XPSC (1S)	284.80	C-C,C-H	81.89	83.67	78.81	84.47	79.23
	286.20	C-O	5.60	7.74	7.90	7.34	8.23
	287.50	C=O	4.36	3.28	7.39	2.65	9.53
	289.50	OH	8.14	5.30	5.89	5.54	3.01
XPSO (1S)	531.50	C=O	29.44	31.41	19.47	26.10	35.78
	532.50	C-O	48.76	40.20	42.51	43.01	47.17
	533.50	OH	21.80	28.40	38.02	30.89	17.05
XPSN (1S)	398.80	Pyridine N	48.86	21.62	41.21	33.50	37.56
	400.20	Pyrrole N	36.88	36.65	12.05	40.38	23.11
	401.20	Quaternary N	3.91	35.37	11.51	11.68	7.12
	402.90	Nitrogen oxides	10.36	6.36	35.23	14.45	32.21
XPSS (2P)	163.16	Mercaptan and thiophenol	20.54	43.45	7.16	8.94	36.93
	164.27	Thiophenic S	28.87	18.99	32.74	28.83	9.64
	165.37	Sulfoxide S	11.58	18.99	14.62	28.89	36.96
	167.67	Sulfone S	10.07	13.75	14.63	16.92	6.82
	168.32	Inorganic S	28.94	4.82	30.85	16.42	9.66

method and the optimization results are displayed in Fig. 7.

3.2. Discussion

In the software, the surface areas of the molecular structures of PDS, HB, XG, CP, and SH were 1328.87 $Å^2$ / molecular structure, 2563.07 $Å^2$ / molecular structure, 2680.883 $Å^2$ / molecular structure, 2831.90 $Å^2$ / molecular structure, and 2840.95 $Å^2$ / molecular structure, respectively, by using an N_2 probe with a radius of 0.184 nm on the solvent

Table 9. Main forms of heteroatoms.

Assignment	Coal sample								
	pyridine N	pyrrole N	quaternary N	Nitrogen oxides	C=O	C-O	OH	N atoms numbers	O atoms numbers
PDS	1	-	-	-	1	2	1	1	4
HB	1	1	1		3	4	3	3	10
XG	2	-	-	2	2	4	4	4	10
CP	2	2	-	-	2	4	3	4	9
SH	2	-	-	2	3	4	2	4	9

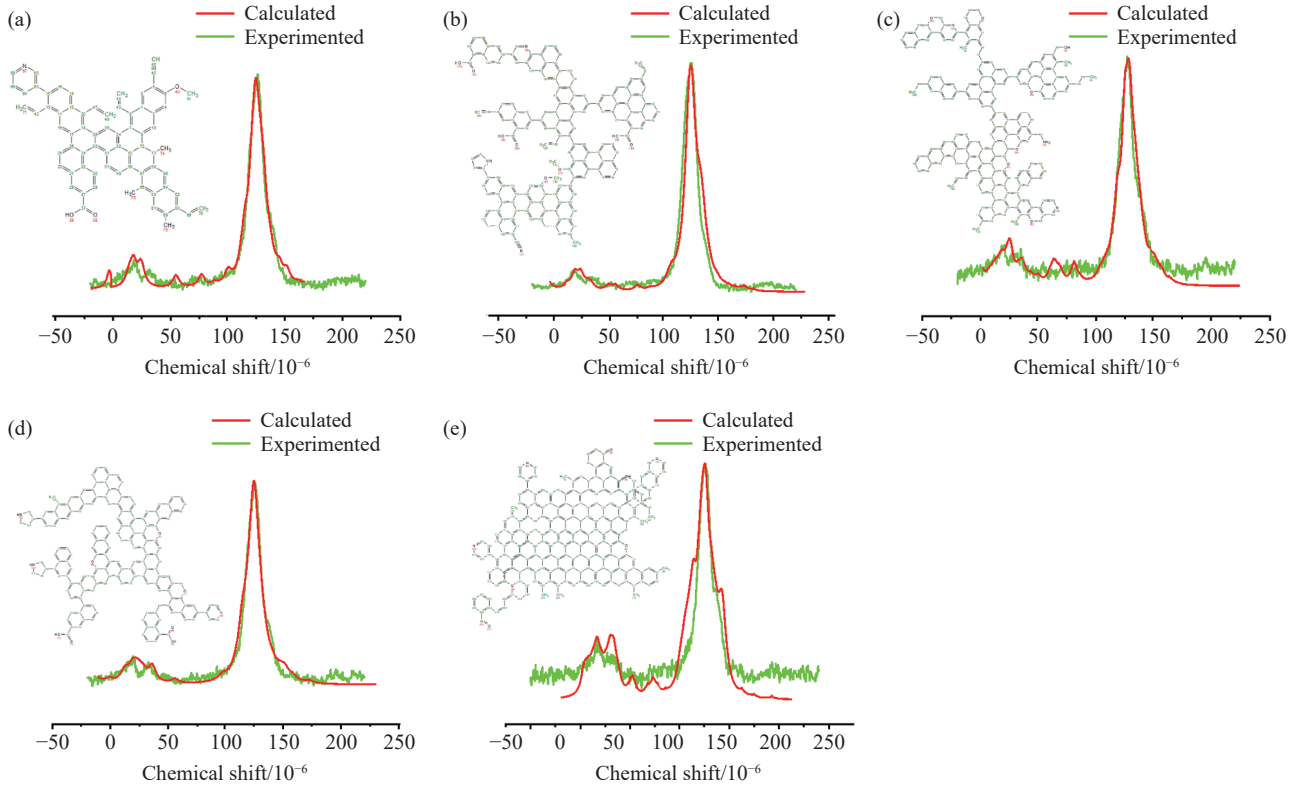

Fig. 6. Planar model and spectra comparison. a–PDS molecular structures model and ^{13}C NMR spectra; b–HB molecular structures model and ^{13}C NMR spectra; c–XG molecular structures model and ^{13}C NMR spectra; d–CP molecular structures model and ^{13}C NMR spectra; e–SH molecular structures model and ^{13}C NMR spectra.

Table 10. Planar macromolecular structure model parameters.

Coal sample number	Simulation Element content	Element analysis test results	Molecular formula	Molecular mass
PDS	C(88.59%)H(5.06%)N(1.43%)O(4.92%)	C(88.98%)H(3.88%)N(1.82%)O(4.82%)	$C_{72}H_{49}NO_3$	976
HB	C(88.32%)H(4.15%)N(1.86%)O(5.67%)	C(88.25%)H(4.29%)N(1.66%)O(5.34%)	$C_{166}H_{93}N_3O_8$	2257
XG	C(89.12%)H(4.89%)N(1.63%)O(4.35%)	C(89.25%)H(4.05%)N(1.73%)O(4.60%)	$C_{191}H_{125}N_3O_7$	2574
CP	C(88.65%)H(4.62%)N(1.84%)O(4.89%)	C(88.91%)H(3.77%)N(1.91%)O(4.98%)	$C_{169}H_{105}N_3O_7$	2289
SH	C(90.52%)H(4.23%)N(1.43%)O(3.82%)	C(91.06%)H(3.13%)N(1.58%)O(3.71%)	$C_{221}H_{123}N_3O_7$	2932

surface. As shown in Fig. 8, the surface area of coal molecular structure increased with the increase of coal rank, and the surface area increased faster when volatile bituminous coal was either a medium-volatility bituminous coal or low-volatility bituminous coal.

In the optimization of the molecular structures, the total energy E is composed of the valence-electron energy E_V and the non-binding energy E_N. The former consists of the bond-stretching energy E_B, bond-angle energy E_A, torsional energy E_T, and inversion energy E_I; the latter mainly includes van der Waals energy E_{van}, Coulombic energy E_E, and hydrogen-bond energy E_H. Changes in the energy are displayed in Table 11.

As Table 11 shows, in the molecular structure model of the coal samples, the non-binding energy E_N is always higher than the valence-electron energy E_V and the former is the main component of the potential energy. This indicates that the stability of the structure model is mainly contributed by the non-binding energy E_N, which is dominated by the van der Waals energy E_{van} for the π-π interactions between aromatic rings. The van der Waals energy is the main cause of the reduction of the non-binding energy, to which the hydrogen-bond energy makes no contribution. The Coulombic energy E_E changes (albeit marginally). These results agree well with simulation results obtained by Carlson and Marzec (Marzec A

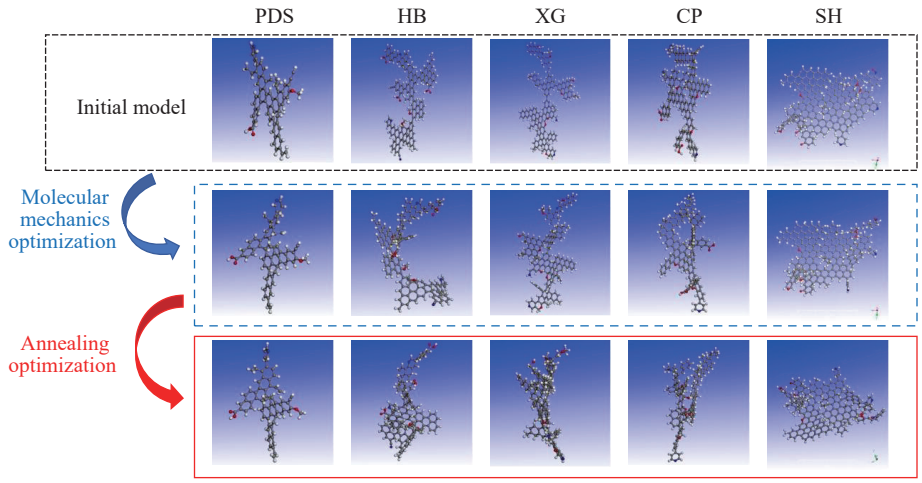

Fig. 7. Comparison diagram of molecular structure model optimization. In the ball-and-stick model, the gray is carbon atoms; the white sphere is hydrogen; the red ball is oxygen; the blue balls are nitrogen atoms.

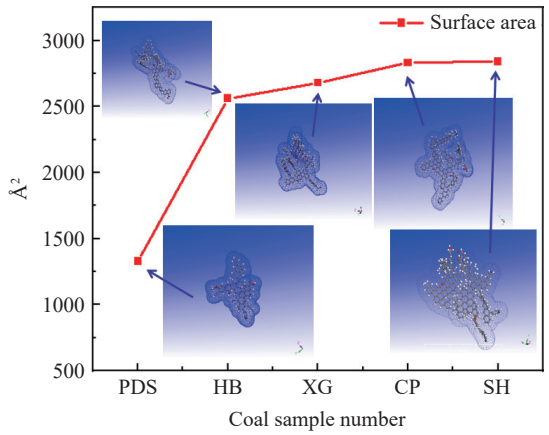

Fig. 8. Surface area analysis diagram.

et al., 2000).

After being optimized, the model of macromolecular structures in coal changes to a significant extent. Bridged bonds and functional groups are twisted, which reduces the valence-electron energy. In the valence-electron energy E_V, the bond-stretching energy exhibits the greatest reduction, which is the main cause of the decrease in the valence-electron energy E_V. The bond-stretching energy E_B determines the compactness of a structure: The greater the energy, the looser the model and *vice versa*. The bond-angle energy E_A decreases in both the HB and XG coal samples, while significantly increases in the PDS, CP, and SH coal samples. Under the condition that R,max% ⩾ 1.78%, the bond-angle energy E_A is in the range of 50–60 kcal/mol, which indicates that E_A gradually stabilizes with increasing degree of metamorphism. The dihedral torsional potential energy E_T shows a large increase, revealing that as the molecular structures in coal change from two-dimensional to three-dimensional with the increasing degree of metamorphism, the structural torsion becomes increasingly apparent. The result implies that the torsion and inversion of bonds and the changes in the bond angle and length are the basis for macromolecules in coal to have a spatial configuration.

Table 11. Structural model optimization energy analysis.

Coal sample number	Optimized conditions	E/(kcal/mol)	E_V/(kcal/mol)				E_N/(kcal/mol)		
			E_B	E_A	E_T	E_I	E_H	E_{Van}	E_E
PDS	Initial structure	4365.63	1365.42	7.50	55.69	1.36	0.00	2924.54	11.13
	Molecular mechanical optimization	328.27	36.10	19.06	78.82	0.97	0.00	182.39	10.93
	Molecular dynamics optimization	329.30	35.51	16.14	79.09	0.81	0.00	181.47	16.28
HB	Initial structure	8458.22	4648.34	141.51	101.50	1.85	0.00	3563.51	1.52
	Molecular mechanical optimization	702.35	85.66	66.78	103.41	3.05	0.00	448.53	−5.08
	Molecular dynamics optimization	665.33	83.68	59.51	116.40	3.46	0.00	409.56	−7.29
XG	Initial structure	10716.67	4977.95	233.39	65.24	2.50	0.00	5421.61	15.98
	Molecular mechanical optimization	850.16	102.13	58.02	141.59	2.55	0.00	524.07	21.81
	Molecular dynamics optimization	811.59	97.00	48.96	146.63	3.52	0.00	490.52	24.96
CP	Initial structure	10529.74	2738.35	32.49	82.82	2.17	0.00	7669.85	4.06
	Molecular mechanical optimization	699.63	86.20	49.29	104.71	2.37	0.00	456.01	1.05
	Molecular dynamics optimization	693.02	85.58	50.16	101.37	1.38	0.00	447.11	7.41
SH	Initial structure	12645.89	3657.32	28.85	128.21	3.66	0.00	8818.84	9.00
	Molecular mechanical optimization	921.55	115.61	55.30	125.24	2.97	0.00	617.68	4.75
	Molecular dynamics optimization	926.29	115.71	55.07	123.25	2.86	0.00	617.54	11.87

3.3. Uncertainty analysis

(i) In the process of establishing the molecular structure model of coal, due to the small content of S element and ignoring its influence on molecular structure, the results of macromolecular structure reconstruction of coal are different from the actual ones to a certain extent.

(2) When using ACD/ChemSketch software to predict ^{13}C NMR data, the experimental spectra and the simulated spectra are only relatively similar, but not completely consistent in accuracy.

4. Conclusions

(i) Using the analysis and detection technology of elemental analysis + FTIR + ^{13}CNMR+XPS, and applying the Origin peak fitting technology and the principle of energy minimum, the construction method of coal molecular structure model of "determination of key structures in coal, construction of planar molecular structure model, and optimization of three-dimensional molecular structure model" was formed.

(ii) The elemental analysis, ^{13}C NMR, FTIR, and XPS test results showed that the proportion of multi-substituted aromatic rings decreased with increasing degree of coal metamorphism. Monozoal aromatic rings accounting for 11.81% appeared in SH anthracite, indicate that the high substituted aromatic rings tended to migrate to the middle and low substituted aromatic rings. With the increase of coal rank, the CH content decreased from 27.27% to 16.24%, the CH_2 content increased from 24.32% to 31.18%, and the CH_3 content increased from 48.41% to 52.58%. This phenomenon was mainly caused by the cyclization of the aliphatic chain, aromatization of the cycloalkane, substitution of the locator group on the aromatic ring, and decarboxylation of the aromatic ring.

(iii) The stability of the structural model of the coal sample is mainly due to the contribution of van der Waals force energy E_{van} in the non-bonding energy E_N, which is dominated by the π-π interaction between aromatic rings, and the hydrogen bonding energy does not contribute. The E_B reduction of key telescopic energy is second only to Van der Waals E_{van}, which is the main controlling factor for the decline of valence electron energy E_V. With the increase of coal metamorphism, the bond angular energy E_A gradually tends to be fixed. During the process of changing the model from 2D to 3D, the structural torsion occurs and the dihedral torsional potential energy E_T becomes stronger and stronger. The torsion, inversion and changes of bond angle and bond length are the basis for the three-dimensional configuration of coal macromolecules.

CRediT authorship contribution statement

Xiao-ming Ni: Writing-reviewing and editing; Jing-shuo Zhang: Conceptualization, methodology, writing original draft preparation, visualization. Xiao-kai Xu: Conceptualization, supervision. Bao-yu Wang: Visualization, investigation. All authors discussed the results and contributed to the final manuscript.

Declaration of competing interest

The authors declare no conflicts of interest.

Acknowledgment

This study was supported by the National Natural Science Foundation of China（41872174 and 42072189） and the Program for Innovative Research Team (in Science and Technology) in the Universities of Henan Province, China (21IRTSTHN007) and the Program for Innovative Research Team (in Science and Technology) of Henan Polytechnic University (T2020-4).

References

Chermin HAG, Van Krevelev DW. 1957. Chemical structure and properties of coal. XVII-A mathematical model of coal pyrolysis. Fuel, 36(1), 85–104.

GB/T 482-2008 Sampling of coal seams, 2008 (in Chinese).

GB/T 482-2008 Method of determining microscopically the reflectance of vitrinite in coal, 2008 (in Chinese).

GB/T 6040-2002 General rules for infrared analysis, 2002 (in Chinese).

GB/T19500-2004 General rules for X-ray photoelectron spectroscopic analysis method, 2004 (in Chinese).

Ge T, Li Y, Wang M, Li F, Zhang MX. 2020. Structural characterization and molecular model construction of gas-fat coal with high sulfur in Shanxi. Spectroscopy and Spectral Analysis, 40(11), 3373–3378. doi: 10.3964/j.issn.1000-0593(2020)11-3373-06.

Given PH. 1960. The distribution of hydrogen in coals and its relation to coal structure. Fuel, 39(2), 147.

Grzybek T, Pietrazk R, Wachowsk H. 2002. X-ray photoelectron spectroscopy study of oxidized coals coals with different sulphurcontent. Fuel Process Technol, 77, 1–7.

Han F, Zhang YG, Meng AH. 2014. FTIR analysis of Yunnan Lignit. Journal of China Coal Society, 39(11), 2293–2299 (in Chinese with English abstract).

Hao PY, Meng YJ, Zeng FG, Yan TT, Xu GB. 2020. Quantitative study of chemical structures of different rank coals based on infrared spectroscopy. Spectroscopy and spectral analysis, 40(3), 787–792. doi: 10.3964/j.issn.1000-0593(2020)03-0787- 06. doi: 10.3964/j.issn.1000-0593(2020)03-0787-06.

Jawad AH, Ismail K, Ishak MAM, Wilson LD. 2019. Conversion of malaysian low-rank coal to mesoporous activated carbon: Structure characterization and adsorption properties. Chinese Journal of Chemical Engineering, 27(7), 1716–1727. doi: 10.1016/j.cjche.2018.12.006.

Jiang JY, Yang WH, Cheng YP, Liu ZD, Zhang Q, Zhao K. 2019. Molecular structure characterization of middle-high rank coal via XRD, Raman and FTIR spectroscopy: Implications for coalification. Fuel, 239, 559–572. doi: 10.1016/j.fuel.2018.11.057.

Kozlowski M. 2004. XPS study of reductively and non-reductively modified coals. Fuel, 83(3), 259–265. doi: 10.1016/j.fuel.2003.08.004.

Li X, Zeng FG, Wang W, Dong K, Cheng LY, 2015. FTIR characterization of structural evolution in low-midlle rank coals. Journal of China Coal Society, 40(12), 2900–2908. doi: 10.13225lj.cnki.jccs.2015.1085.

Li W, Zhu YM, Wang G, Jiang B. 2016. Characterization of coalification jumps during high rank coal chemical structure evolution. Fuel, 185, 298–304. doi: 10.1016/j.fuel.2016.07.121.

Liu Y, Zhu YM, Li W, Zhang CH, Wang Y. 2017. Ultra micropores in macromolecular structure of subbituminous coal vitrinite. Fuel, 210, 298–306. doi: 10.1016/j.fuel.2017.08.069.

Liu WY, Liu QF, Liu LS, Liu D. 2019. Study on FTIR features of middle and high rank coal structure in north part of Qinshui Basin. Journal of Coal Science and Technology, 47(2), 181–187. doi: 10.13199/j.carolcarrollnkiCST.2019.02.030.

Liu BJ, Chu GC, Zhao CL, Sun YZ. 2022. Leaching behavior of Li and Ga from granitic rocks and sorption on kaolinite: Implications for their enrichment in the Jungar Coalfield, Ordos Basin. China Geology, 5(1), 34–45. doi: 10.31035/cg2021024.

Marzec A. 2000. Intermolecular interactions of aromatic hydrocarbons in carbonaceous materials a molecular and quantum mechanics. Carbon, 38(3), 1863–1871.

Metrological Specifications of the People's Republic of China. 2011. JJF1321-2011 Calibration Specification for Elemental Analyzers.

Ping A, Xia W, Peng Y, Xie GY, 2020. Construction of bituminous coal vitrinite and inertinite molecular assisted by ^{13}C NMR, FTIR and XPS. Journal of Molecular Structure, 1222, 128959. doi: 10.1016/j.molstruc.2020.128959.

Shinne JH. 1984. From coal to single stage and two-stage products: A reactive model of coal structure. Fuel, 63(9), 1187–1196. doi: 10.1016/0016-2361(84)90422-8.

Song Y, Zhu YM, Li W, 2017. Macromolecule simulation and CH_4 adsorption mechanism of coal vitrinite. Applied Surface Science, 396, 291–302. doi: 10.1016/j.apsusc.2016.10.127.

Surip SN, Ahmed Saud A, Zaharaddeen NG, Syed SA, Syed-Hassan KI, Ali HJ. 2020. H_2SO_4-treated malaysian low rank coal for methylene blue dye decolourization and COD reduction: Optimization of adsorption and mechanism study. Surfaces and Interfaces, 21, 100641. doi: 10.1016/j.surfin.2020.100641.

Jia TG, Li X, Qu GN, Li W, Yao HF, Liu TF. 2021. FTIR characterization of chemical structures characteristics of coal samples with different metamorphic degrees. Spectroscopy and Spectral Analysis, 41(11), 3363–3369. doi: 10.3964/j.issn.1000-0593(2021)11-3363-07.

Wiser WH. 1975. Reported in division of fuel chemistry. Preprints, 20(1), 122.

Xiang JH, Zeng FG, Liang HZ, Ll MF, SONG XX, ZHAO YY. 2016. Carbon structurecharacteristics and evolution mechanism of coal with different metamorphic degrees. Journal of China Coal Society, 41(6), 1498–1506 (in Chinese with English abstract).

Xie HP, Wang JH, Wang GF, Ren HW, Liu JZ, Ge SR, Zhou HW, Wu G, Ren SH. 2018. The new concept of coal revolution and the conception of coal science and technology development. Journal of China Coal Society, 43(5), 1187–1197 (in Chinese with English abstract).

Yan JH, Lei ZP, Li ZK, Wang ZC, Ren SB, Kang SG, Wang XL, Shui HF, 2020. Molecular structure characterization of low-medium rank coals via XRD, solid state ^{13}C NMR and FTIR spectroscopy. Fuel, 268, 117038. doi: 10.1016/j.fuel.2020.117038.

Zhao YG, Li MF, Zeng FG. 2018. FTIR study of structural characteristics of different chemical components from Yimin Lignite. Journal of China Coal Society, 43(2), 546–554 (in Chinese with English abstract).

Zhou XY, Zeng FG, Xiang JH, Deng XP, Xiang XH. 2020. Macromolecular model construction and molecular simulation of organic matter in Majiliang vitrain. CIESC Journal, 71(4), 1802–1811 (in Chinese with English abstract).